

# Sound-speed measurements near the ocean surface

Eric Lamarre<sup>a)</sup>

*R. M. Parsons Laboratory, Department of Civil & Environmental Engineering, Massachusetts Institute of Technology, Cambridge, Massachusetts 02139 and Woods Hole Oceanographic Institution, Woods Hole, Massachusetts 02543*

W. K. Melville

*Scripps Institution of Oceanography, University of California San Diego, LaJolla, California 92093-0213 and R. M. Parsons Laboratory, Department of Civil & Environmental Engineering, Massachusetts Institute of Technology, Cambridge, Massachusetts 02139*

(Received 23 September 1993; accepted for publication 17 December 1993)

The results of two field experiments conducted in the fall of 1992 on the measurement of sound speed near the ocean surface are reported. The measurement technique makes use of the travel time of short acoustic pulses between a transmitter and a receiver separated by 40 cm [Lamarre and Melville, *J. Atmos. and Oceanic Tech.* (1994)]. The instrument is capable of making simultaneous measurements of the sound speed at six depths, starting at 0.5 m, over a frequency range from 5 to 40 kHz. Time series of sound speed show dramatic fluctuations over time periods on the order of minutes or less. These are attributed to the formation of bubble plumes or the passage of bubble clouds. In two particular instances, a newly created bubble plume generated a sound-speed reduction of 800 m/s at a depth of 0.5 m; and a bubble cloud 25-s old generated a reduction of 400 m/s. Frequent occurrences of sound-speed reductions greater than 100 m/s are observed during moderate wind conditions (8 m/s). The signals at various depths are highly correlated and mostly coherent at frequencies below 0.05 Hz. The time-averaged (20 min) sound-speed profile is found to be significantly more pronounced and shallower than previously reported. The average sound-speed reduction is found to correlate with wind speed. Simultaneous measurements at several acoustic frequencies show that the sound speed is nondispersive below 20 kHz for moderate wind conditions of up to 8 m/s. Upward-looking sonar data reveal the presence of bubble clouds which correlate with the large sound-speed reductions observed. However, even though bubble clouds are present down to a depth of 3 m and greater, significant sound-speed reductions are confined to the first meter below the surface.

PACS numbers: 43.30Es, 43.30.Nb

## INTRODUCTION

Air bubbles are entrained into the water column by the breaking of surface waves. Although some bubbles have been observed down to a depth of  $O(10\text{ m})$ , usually they are located within one or two meters of the surface.<sup>1-3</sup> Air bubbles have been found to form distinct plumes and clouds which are the results of breaking waves and Langmuir circulations.<sup>1,2,4</sup> These bubble plumes and clouds are believed to be responsible for the high levels of acoustic reverberation observed at the ocean surface at wind speeds in excess of 10 m/s.<sup>5</sup> Air bubbles also have an important role to play in the dynamics of the ocean's surface layer because of their ability to increase the effective transfer rate of heat and gases between the atmosphere and the ocean.<sup>1,6,7</sup>

In the presence of bubbles, the velocity of sound in water can change significantly from its bubble-free value of approximately 1500 m/s. At frequencies below bubble resonance, the sound velocity is controlled by the total volume fraction of air in the water (hereafter void fraction). In fact,

void fraction and sound speed at low frequencies are related through Wood's<sup>8</sup> equation with void-fractions in the range  $10^{-6}$  to  $10^{-2}$  corresponding to sound-speed reductions in the range 100 to 1400 m/s, respectively. These sound-speed reductions are very large compared to fluctuations caused by changes in temperature, salinity or density which typically range from a few to tens of meters per seconds and vary on comparatively longer time scales of the order hours and longer.

At frequencies near bubble resonance, the propagation velocity is dominated by phase shifts introduced by bubbles. The sound-speed becomes faster or slower depending on whether the acoustic frequency is slightly above or below the bubble resonance frequency. For a bubble population of uniform size, the sound-speed departures can be very large [ $O(1000\text{ m/s})$ ]. For a mixture of bubbles of various sizes, as found in the upper-ocean, the sound-speed departures are significantly reduced since an increase in the sound velocity caused by bubbles whose resonance frequency is slightly below the frequency of the sound wave is offset by a decrease caused by bubbles whose resonance frequency is slightly above. At frequencies well above bubble resonance, the sound velocity returns to its bubble-free value. The attenua-

<sup>a)</sup>Present affiliation: Collège des Ingénieurs, 49 rue de l'Université, 75007 Paris, France.

tion of sound waves propagating through a bubbly mixture is most important at frequencies matching the resonance of the bubbles. Away from bubble resonances, the attenuation diminishes. A more detailed presentation of the dispersion and attenuation effects caused by bubbles can be found in Clay and Medwin<sup>9</sup> and in Commander and Prosperetti.<sup>10</sup>

Sound is a powerful tool which can be used to remotely monitor upper-ocean processes. For example, passive techniques include the monitoring of wind speeds<sup>11</sup> and rainfall rates<sup>12,13</sup> over the oceans and the detection of breaking waves.<sup>14</sup> It is also hoped that in the near future we may be able to remotely sense the dissipation of surface wave energy by breaking<sup>15-17</sup> and the transfer rates of gases across the air-sea interface.<sup>18</sup> However, many of the benefits offered by acoustic remote sensing near the ocean surface depend on prior knowledge of the propagation characteristics between the source (near or at the surface) and the receiver located at some depth below the surface.<sup>19</sup> Without this information, it is difficult to separate acoustic features that are caused by the source from those caused by the medium through which the sound must propagate. Since the rough water surface and the air bubbles below it dominate the nature of sound propagation near the surface; it is necessary to have a good description of the spatial and temporal changes in the sound speed and attenuation field within the bubbly region.

Only a few studies have been conducted on the measurement of sound speed near the ocean surface. Medwin and his co-authors made measurements of sound-speed fluctuations near the surface with a cw signal transmitted between two horizontal hydrophones at various frequencies in the range 15 to 100 kHz.<sup>20,21</sup> The sound speed was computed by measuring phase shifts at sea and by comparing them to a reference phase shift in bubble-free water. Their instrument had a resolution of 0.1 m/s but it was limited to a minimum measurement depth of 3 m in order to minimize surface reflections which would have corrupted the phase. Their results showed maximum sound-speed reductions on the order of 10 to 15 m/s at depths greater than 3 m during light wind conditions. These suggest that higher values are likely to be found closer to the surface. However, these measurements were taken from offshore platforms where the bubble densities are greater due to increased breaking on the structure of the platforms. It is likely that for similar wind speeds, measurements away from offshore platforms would yield smaller sound-speed reductions. Finally, these studies also showed that the sound speed was nondispersive below 25 kHz at 5 m depth for wind speeds of approximately 5 m/s.

Farmer and Vagle<sup>2</sup> used a multifrequency upward looking sonar to measure the bubble density at four discrete bubble sizes (16, 37, 65, and 116  $\mu\text{m}$ ) at depths ranging from 0.1 to 10 m. From these measurements, they inferred the shape of the bubble size distribution. They computed the time-averaged sound-speed profiles by integrating the dispersive effects of all bubbles using a known integral equation which takes as input the bubble size distribution.<sup>9</sup> Their data showed that sound-speed reductions are the largest at the surface (3 to 15 m/s) for wind conditions between 10 and 12 m/s and decrease exponentially with depth with an  $e$ -folding depth of approximately 1.4 m. It should be pointed out that

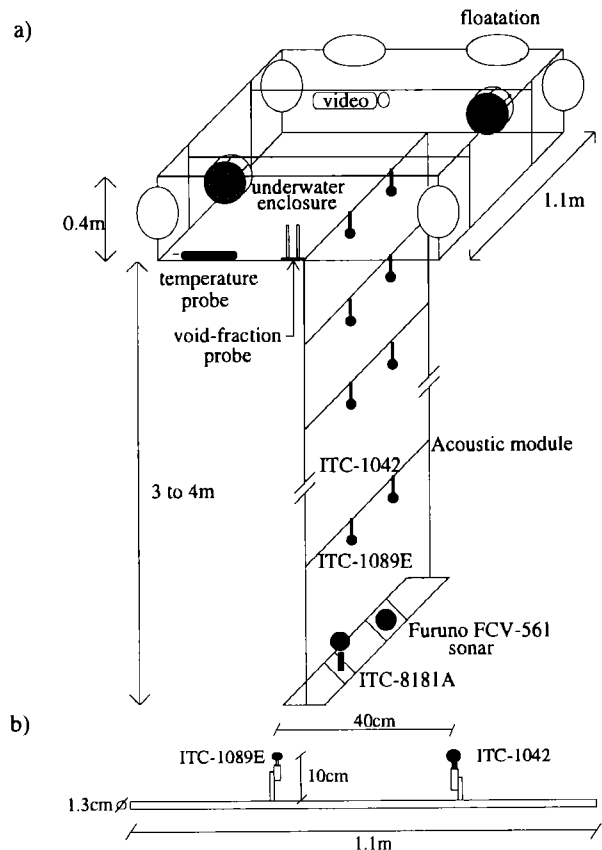


FIG. 1. (a) Sketch of the buoy and its instrumentation. (b) Sketch of the hydrophone support module.

sound-speed calculations based on integration of bubble population data are very sensitive to the exact shape of the bubble population and the location of its upper and lower limits for which there are still large discrepancies in the literature (see Sec. IV).

The measurements of sound speed by Medwin and his co-authors<sup>20,21</sup> were limited to a minimum depth of 3 m and a minimum frequency of 15 kHz. Farmer and Vagle's<sup>2</sup> measurements had the distinct advantage of being nonintrusive but they were impeded by the difficulties in computing the sound velocity from bubble population data and by the limitations of echo sounders in regions of large void fractions (see Sec. IV). Furthermore, the above studies have focused on a time-averaged [ $O(10 \text{ min})$ ] description of the sound speed and little has been done to describe the short term fluctuations. In this paper, we report on direct and simultaneous measurements of sound speed at six different depths with the shallowest one being 0.5 m, over a frequency range from 5 to 40 kHz.

## I. THE EXPERIMENTS

### A. The instrumentation

The instrumentation and the technique are described in detail in separate papers.<sup>22,23</sup> Here we only give a brief overview. A light buoy was built to carry the probes and instrumentation [Fig. 1(a)]. The buoy was equipped with six acoustic sound-speed measuring modules. Each module in-

cluded a transmit and a receive omnidirectional hydrophone both rigidly supported on a stainless-steel rod [Fig. 1(b)]. The transmit hydrophone was an ITC-1042 and the receive hydrophone was an ITC-1089E. Other instrumentation on the buoy included a Sea-Bird SBE 3 temperature sensor which was used to calculate the speed of sound in bubble-free water. An NEC TI-23A video camera mounted inside a Video Vault (Spring, Texas) underwater housing was used to image the bubble plumes and clouds formed at or near the buoy. From the video measurements, it was found that the buoy tracked the water surface to within  $\pm 10$  cm. An 88-kHz Furuno model FCV-561 upward looking sonar was mounted at the bottom of the buoy. The sonar was used to image the bubble clouds as has been previously done by Thorpe<sup>1</sup> and Farmer and Vagle<sup>2</sup> among others. Two 150-m underwater multiconductor cables served as links between the sensors on the buoy and the instrumentation on board the ship. The cables were connected to two underwater enclosures mounted on the buoy. The enclosures served as junction boxes between the buoy probes and the multiconductor cables. The buoy was tethered from a ship and the ship was maneuvered to keep the tether slack at all times, and the buoy clear of the ship's wind and wave wakes.

The sound-speed measurement technique is based on estimating the travel time (or time delay) of an acoustic pulse as it propagates from a transmitter to a receiver separated by 40 cm. Phase distortions caused by acoustic reflections from the surface or from nearby structural buoy elements are separated in time from the direct path signal. A DSP-based data processing system was implemented to cross correlate the transmitted and received acoustic pulses and thus yield time-delay and sound-speed measurements in real time. Perhaps the most significant novelty of the present measurement technique is its ability to make simultaneous measurements of the sound speed at several depths (6), starting as close as 0.5 m to the surface, over the acoustic frequency range from 5 to 40 kHz at a rate of 4 Hz at each depth. Furthermore, the technique for measuring the speed of sound is a direct one which avoids the many difficulties involved with inferring the sound speed from *in situ* void fraction or bubble population measurements. This advantage is made clear by the fact that very small values of void fraction [say  $O(10^{-4})$ ] lead to  $O(1)$  changes in the speed of sound. The instrumentation was thoroughly tested in a laboratory and in a lake against known sound-speed variations.<sup>22,23</sup>

## B. The experimental sites

The first experiment was conducted during the first week of October 1992 from the R/V SPROUL off the coast of California near San Diego. The winds were relatively weak during the period of this experiment and therefore it was decided to position the ship in the Santa Cruz Channel, between the islands of Santa Cruz and Santa Rosa, in order to benefit from the wind-tunneling effect caused by the topography of these islands. The maximum steady wind speed recorded by the ship's anemometer for the entire period of the experiment was approximately 8 m/s. Thus the wind conditions for the San Diego experiment varied from very calm to moderate, and the waves were fetched limited by the 12

km length of the Santa Cruz Channel. The water depth in the channel is approximately 60 m. For this experiment, we report on the results from approximately 7 h of data acquired in the Santa Cruz Channel and 3 h acquired at other positions along the California coast in very calm sea states (wind speeds less than 3 m/s).

The second experiment was conducted during the first two weeks of November 1992 from the R/V ASTERIAS in Buzzards Bay, Massachusetts. The purpose of the experiment was to complement the data set acquired during the San Diego experiment with data at higher wind speeds ( $U \geq 8$  m/s). Accordingly, the ship only made short day trips into Buzzards Bay when the wind conditions were sufficiently high. Unfortunately, the wind conditions for the two weeks of the experiment were not higher than 8 m/s (steady) and therefore the data set for the Buzzards Bay experiment is limited to 5 h of data at winds varying between 6 to 8 m/s with significant wave heights (SWH) from 0.2 to 0.65 m. All of the measurements reported from this experiment were acquired close to the Buzzards Bay light tower at the entrance to the bay where the water depth is approximately 20 m. A MiniSpec wave height sensor (Coastal Leasing, Cambridge, MA) was suspended between two legs of the tower in order to measure the wave height.

## II. THE EXPERIMENTAL PROCEDURE

On a typical deployment, the buoy and its instrumentation were kept approximately 100 to 130 m from the ship and the boat was maneuvered such that the buoy was abeam the ship as much as possible. Thus the ship's wake was kept away from the buoy. The tether was constantly monitored and kept slack by maneuvering the boat accordingly. Hence, the buoy was effectively drifting under its own drag and the drag of the cable and floats that linked it to the ship. It should be pointed out that the length and draft of the R/V SPROUL were 38 and 2.9 m, respectively, while those of the R/V ASTERIAS were 14 and 1.4 m, respectively. Thus, since the separation between the ship and the buoy was significantly longer than the dimensions of the ships, we expect that interference from the ships was negligible.

The deployments generally lasted from 1 to 3 h and during that time, the sound-speed profiles were measured at different frequencies for a period of 10 to 20 min at each frequency. The selected frequencies were 5, 7.5, 10, 15, and 20 kHz for the San Diego experiment. For the Buzzards Bay experiment, 5 and 10 kHz were used along with a broadband pulse signal (see below) covering a frequency range from 6 to 40 kHz. The sound speed was processed at a rate of 2 Hz at each depth and a small fraction of the data set was processed at the maximum rate of 4 Hz. The time series were composed of continuous 80-s data segments separated by 10-s gaps during which the raw data (acoustic pulses) and the processed data (time delays) were written to optical disk. In the presentation of the results, the small 10-s gaps are ignored when plotting 20-min time series but are taken into account in the data processing and they are displayed when plotting shorter time segments.

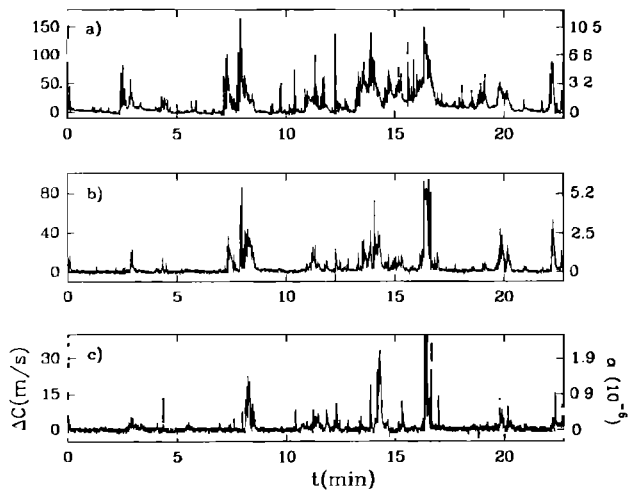


FIG. 2. Sound-speed anomalies at depths (a) 0.5 m, (b) 0.75 m, and (c) 1.0 m. Note the different vertical axes for all three plots. The axes on the right-hand side show the corresponding void-fraction. The frequency of the acoustic pulses was 10 kHz. The wind speed and the SWH were 8 m/s and 0.45 m, respectively. Sampling rate was 2 Hz/ch. Buzzards Bay data.

### III. RESULTS

#### A. Time series and signal characteristics

The sound-speed anomaly is defined as  $\Delta c = c_w - c$  where  $c_w$  and  $c$  are the speed of sound in bubble-free water and in the bubbly mixture, respectively. The bubble-free sound speed  $c_w$  is obtained from measurements at sea during very calm conditions when there is no breaking. Note that the water temperature is continuously recorded during the experiment in order to compensate for the variations of  $c_w$  with temperature.<sup>24,25</sup> The knowledge of  $c_w$  therefore permits the computation of  $\Delta c$  from measurement of the sound speed.

Figure 2 shows time series of the sound-speed anomaly for 10-kHz acoustic pulses taken simultaneously at depths of 0.5, 0.75, and 1.0 m. The signals at different depths are clearly correlated which would suggest that fluctuations are caused by well-defined bubble clouds which pass by the sensors. The magnitude of the anomalies is also found to rapidly decrease with depth which is consistent with the fact that the bubble density is expected to be the highest near the surface. Because of the moderate wind conditions, the occurrences of large excursions in the signal are relatively infrequent and usually followed by periods where the signal returns back to the noise level. The fluctuations themselves are typically very large and they clearly dominate the long-term average at all depths. Note that the corresponding void-fraction based on Wood's<sup>8</sup> equation is shown on the vertical axis on the right-hand side. It will be shown in Sec. III E that the sound speed is nondispersive below 20 kHz for moderate wind conditions (8 m/s or below) and thus the use of Wood's equation to infer void fraction is justified for acoustic frequencies below 20 kHz.

The root-mean-square (rms) noise at 10 kHz was calculated to be 0.7 m/s and the peak-to-peak noise level of the measurements is approximately  $\pm 2$  m/s which was consistent with laboratory tests.<sup>22,23</sup> At 5 kHz, the rms noise was

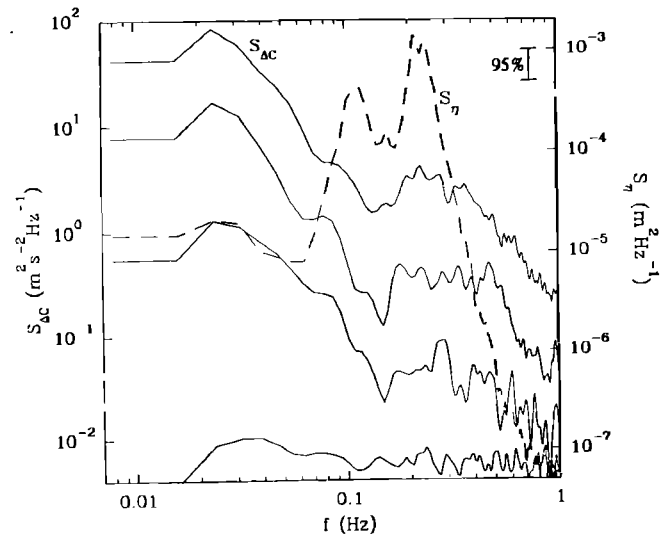


FIG. 3. Solid lines are, from top to bottom, the frequency spectrum of the sound-speed anomalies at 0.5, 0.75, 1.0, and 2.0 m and the dashed line is the frequency spectrum of the waveheight measured at the Buzzards Bay entrance tower. The lowest solid line spectrum (at 2.0 m) is representative of the noise level. Buzzards Bay data.

found to be 2.7 m/s and the peak-to-peak noise approximately  $\pm 5$  m/s. The higher noise level at 5 kHz was caused by ship noise which typically is higher at lower frequencies. For both the Buzzards Bay and the San Diego experiments, we have consistently observed the presence of a signal above the noise level down to a depth of 1.0 m for the highest steady wind conditions attained in both of these experiments (8 m/s). However, very few occurrences of signals above the noise level were observed at a depth of 1.5 m in the entire data set and none at a depth of 2.0 m and greater.

The frequency spectrum of the time series in Fig. 2 was computed along with those of two other 20 min time series taken during the same deployment at the same acoustic frequency and at similar wind speed and significant wave height. The three time series were subdivided into a total of 42 segments of 80 s which were Hanning windowed. The 42 individual spectra were then ensemble averaged to yield the four solid line spectra of Fig. 3 for four different measurement depths. As expected, the energy in the spectra decreases with depth until it reaches the noise level for the lower most spectrum which is for measurements taken at a depth of 2.0 m. For the other three shallower depths, most of the energy in the signal is contained at frequencies much lower than the dominant frequency of the waves. The energy in this low-frequency region is due to the large and relatively slow fluctuations present in the time series and caused by the passage of bubble clouds. Note that the low-frequency peak in the spectra at approximately 0.02 Hz is caused by the use of a short 80-s record length to compute the individual spectrum. Thus, the spectral resolution for frequencies below 0.02 Hz may not be reliable and the peak could be at a lower frequency.

At higher frequencies, there is a distinct peak in the solid line spectra of Fig. 3 at approximately 0.25 Hz. The dashed line in Fig. 3 shows the wave height spectrum measured at the Buzzards Bay light tower which was located never more

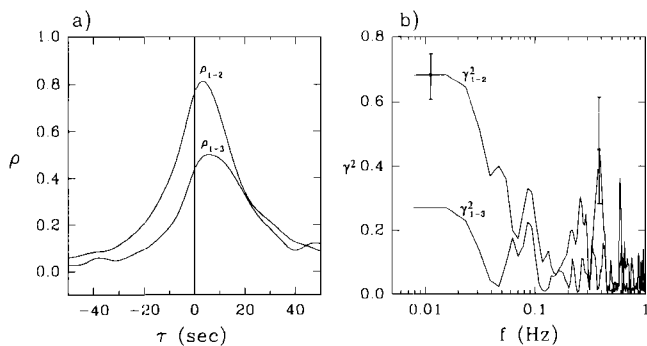


FIG. 4. (a) Correlation coefficient between measurements at 0.5 and 0.75 m ( $\rho_{1,2}$ ); and between measurements at 0.5 and 1.0 m ( $\rho_{1,3}$ ). (b) Coherence between measurement at 0.5 and 0.75 m ( $\gamma_{1,2}^2$ ); and between measurements at 0.5 and 1.0 m ( $\gamma_{1,3}^2$ ). Three 20-min time series were used for both plots (42 records of 80 s). The time series were digitally low-pass filtered at 0.1 Hz for the results shown in (a) in order to eliminate the high-frequency wave-generated signal which is in phase at all depths and which distorted the peak near zero lag. Wind speed and significant waveheight were 8 m/s and 0.45 m, respectively. The 95% confidence interval for two values of the coherence are shown. Buzzards Bay data.

than 3 km away from the ship during the deployments. The peak at approximately 0.25 Hz in the sound-speed anomaly spectra (solid lines) corresponds to the peak of the dominant waves (dashed line). This can be explained by the fact that the buoy response always lags, to some extent, the changes in the wave field and this causes small variations in the vertical and horizontal positions of the sensors with respect to the orbital motion of the water located at the same depth as the sensors. Thus bubble clouds are advected laterally and vertically past the sensors with a velocity due, in part, to the orbital motion of the waves. Even if the buoy were to perfectly follow the water surface, such signals would still be generated because the orbital motion of the wave decays with depth while the sensors maintain a fixed distance from the surface. This effect when combined with spatial inhomogeneities in the sound-speed field will always lead to a signal at surface wave frequencies. It should be pointed out that the above results are not restricted to a 10-kHz acoustic pulse frequency and that similar results were obtained with 5-kHz pulses although the higher noise level at that frequency made it more difficult to detect the wave generated peak in the spectra of the sound-speed anomaly.

The correlation and coherence between measurements realized at different depths were computed for the same three 20-min records used in the spectra of Fig. 3. To facilitate the identification of the various depths on the figures, we adopt the convention that 0.5, 0.75, and 1.0 m correspond to the depth numbers 1, 2, and 3, respectively. Thus the correlation coefficient  $\rho_{1,2}$  is obtained by cross correlating the measurements at 0.5 and 0.75 m. Figure 4(a) shows the correlation coefficient  $\rho$  as a function of the lag  $\tau$  for lags close to zero. The data show that measurements at various depths are significantly correlated and that the correlation diminishes as the distance between the sensors increases. This is mostly due to the fact that the deeper sensors miss the smaller sound-speed anomalies. The data also show that the highest correlations are at some small positive lag which increases with sensor separation. A positive lag corresponds to a de-

layed signal at the deeper sensors. Two possible mechanisms can be suggested for the generation of this lag. The lag could be caused by the finite vertical penetration speed of the bubble plumes entrained by breaking waves. The lag could also be caused by the shape of the bubble clouds which drift pass the sensors. Indeed, clouds generated by prior breaking events, with a leading edge close to the surface, will also give similar time delay. It is not possible at this time to establish which mechanism is the dominant one.

The coherence shown in Fig. 4(b) shows that measurements at various depths are most coherent at very low frequencies and that the coherence decreases as the separation between the sensors increases. Again, this is explained by the fact that the deeper sensors do not detect many of the smaller sound-speed anomalies. Also notice the relatively high coherence in some frequency bands at the surface wave frequencies near 0.25 Hz.

The probability distribution of the sound-speed anomaly at a depth of 0.5 m for the same three 20-min records is shown in Fig. 5(a). The shape of the distribution is close to exponential except close to zero sound-speed anomaly where the noise of the measurements dominates the distribution and forces it to more closely fit a normal distribution. The data in Fig. 5(a) are plotted again on a log-linear scale in Fig. 5(b) along with data at three other depths. The distribution at a depth of 2.0 m is representative of the measurement noise. Away from the noise region (say  $\Delta C > 2$  m/s), the distributions at all depths are exponential with the slope of the distributions steepening with depth. This indicates that the sound-speed anomalies above the noise of the instrument are becoming less frequent and of lesser magnitude as the depth increases. The exponential nature of the distributions also indicates that the frequency of occurrence of sound-speed anomalies decreases very rapidly with an increase in the magnitude of the anomaly. The cumulative probability distributions are shown in Fig. 5(c) for the same four depths. The dashed line on the distribution at 0.5 m indicates that 20% of the measurements had anomalies above 27 m/s. Thus although the excursions of the sound-speed anomalies can be very large, the frequency of their occurrence is relatively small.

## B. Dependence of the sound-speed anomaly on depth and wind speed

The three time series in Fig. 2 clearly show that the amplitudes of the sound-speed anomalies decrease with depth. The averages of six 20-min time series obtained at a wind speed of 7 to 8 m/s were computed and plotted as a function of depth in Fig. 6. The data show some scatter but have a distinct trend corresponding to an exponential decrease with depth.

The equation describing the exponential is

$$\overline{\Delta c} = 370 \text{ m/s } e^{-d/0.18 \text{ m}}, \quad (1)$$

where  $d$  is the depth from the free surface. The  $e$ -folding depth of the measurements is 0.18 m and the anomaly extrapolated to the surface is 370 m/s. For comparison, the exponential decrease described by the measurements of Farmer and Vagle<sup>2</sup> at a wind speed of 10 m/s show an

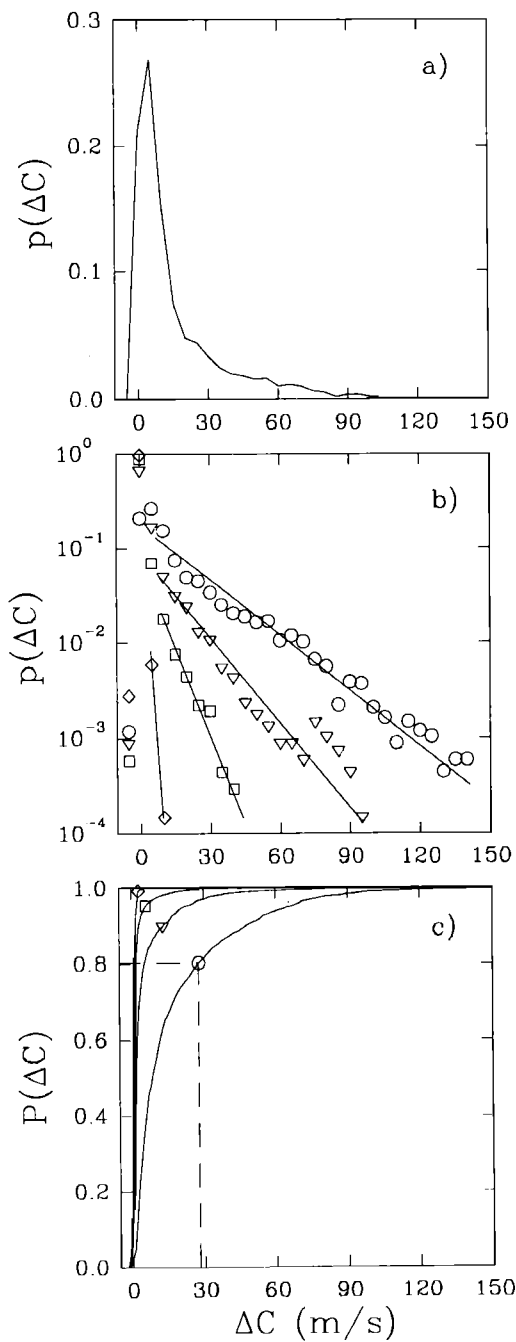


FIG. 5. (a) Probability distribution of the sound-speed anomaly at 0.5 m for three 20-min records ( $f=10$  kHz). The bin size used for the distribution is 5 m/s. (b) Same as in (a) but plotted with results at three other depths on a log-linear scale. The straight lines show the trend of the data away from the noise region. The distribution at 2.0 m is representative of the measurement noise. (c) Cumulative probability distribution corresponding to the distributions in (b). The dashed line in (c) shows that at a depth of 0.5 m, 20% of the data had a sound-speed anomaly greater than 27 m/s. (○) 0.5 m, (▽) 0.75 m, (□) 1.0 m, (◇) 2.0 m depth. Buzzards Bay data.

$e$ -folding depth of 1.4 m and an anomaly at the surface of 3 m/s. Thus there is approximately two orders of magnitude difference in the magnitude of the surface anomaly and one order of magnitude difference in the  $e$ -folding depth between our measurements and those of Farmer and Vagle,<sup>2</sup> with our sound-speed profile being much more pronounced and shallower. These differences are discussed in Sec. IV.

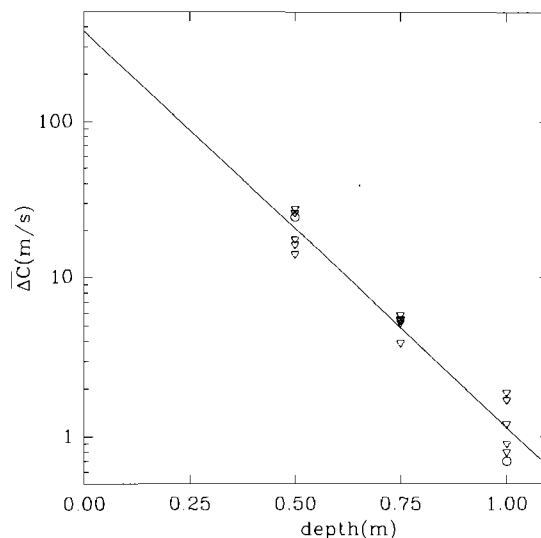


FIG. 6. Average sound-speed anomaly  $\overline{\Delta c}$  as a function of depth. Each data symbol is a 20-min average. (▽) Buzzards Bay experiment and (○) San Diego experiment. The solid line is the best exponential fit to the data. Wind speed of 7 to 8 m/s. The frequency of the acoustic pulses was either 5 or 10 kHz.

Although it may be clear that in general the average sound-speed anomaly increases with wind speed, it is less evident how the probability distribution of the signal may change with a change in wind conditions. Three sets of three 20-min time series were selected to cover a significant range of wind speeds. All data selected were for acoustic frequencies of 10 kHz or less. The probability distributions of the sound-speed anomalies at a depth of 0.5 m for all three data sets (1 h each set) are shown in Fig. 7(a) along with the cumulative distributions in Fig. 7(b). The probability distributions in Fig. 7(a) show an approximately exponential relationship with a slope that steepens with a decrease in wind speed. An interesting feature of the probability distributions at the higher wind speeds is their close match up to 40 m/s after which the slopes diverge. This suggests that the effect of higher wind speed is primarily to increase the frequency of occurrences of large sound-speed anomalies while keeping relatively constant the frequency of occurrence of smaller anomalies. In contrast, the depth dependency of the probability distributions in Fig. 5(a) showed a clear decrease in the

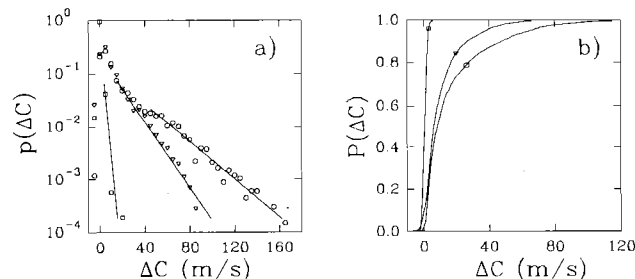


FIG. 7. (a) Probability distribution for three different wind conditions. Each distribution was obtained from three 20-min time series. (○) 7.5 to 8 m/s (Buzzards Bay data), (▽) 5.5 to 6 m/s (San Diego data), (□) less than 3 m/s and representative of the noise level (San Diego data). (b) Cumulative probability distribution for the same data.

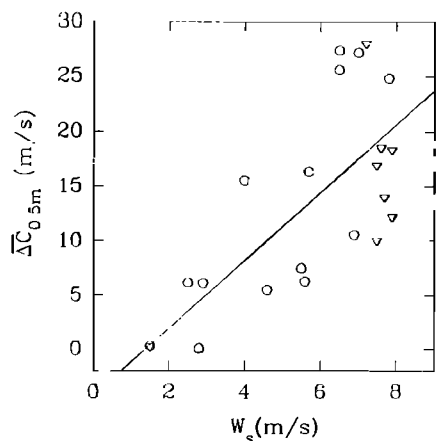


FIG. 8. Average sound-speed anomaly at 0.5-m depth as a function of wind speed. Data were averaged over 20-min records. The solid line is a best linear fit to the data with a 0.74 correlation coefficient. (O) Data from San Diego experiment, ( $\nabla$ ) data from Buzzards Bay experiment.

frequency of occurrences of both small and large anomalies with an increase in depth.

### C. Correlation with environmental parameters

Correlation of the average sound-speed anomalies with wind speed was performed. Only the data at 5 and 10 kHz were selected in order to ensure that the measurements were representative of the low-frequency sound speed (see Sec. III E). The sound-speed data and the environmental data were averaged over 20-min records. Figure 8 shows the average sound-speed anomaly plotted against wind speed. Although the data are correlated, there is nevertheless significant scatter which suggests that an averaging time longer than 20 min should be used to improve the correlation or that other environmental variables are of comparable significance. Measurements of significant waveheights with measurements of sound-speed anomalies were too limited to obtain meaningful correlations.

### D. Highest sound-speed anomaly measured

Figure 9 shows a short time series of the highest sound-speed anomalies measured during the experiments. Notice that the actual sampled data points are shown in order to demonstrate that the high excursions in the signal are not due to single outliers. This particular time period was also recorded by the underwater video camera and two interesting features were viewed on the video recording which help our understanding of the anomalies observed. The underwater camera was equipped with a wide angle lens and was positioned to look horizontally at a depth of approximately 25 cm (details on the camera are given in Lamarre and Melville<sup>4</sup>). Hence, the camera was capable of observing bubble plumes being formed at the buoy and those being formed some distance away as long as they remained in the field of view.

The vertical arrow in Fig. 9(a) corresponds to the beginning of a breaking wave on the video recording. This particular wave broke right above the buoy and injected a large plume of bubbles which were observed to reach the upper-

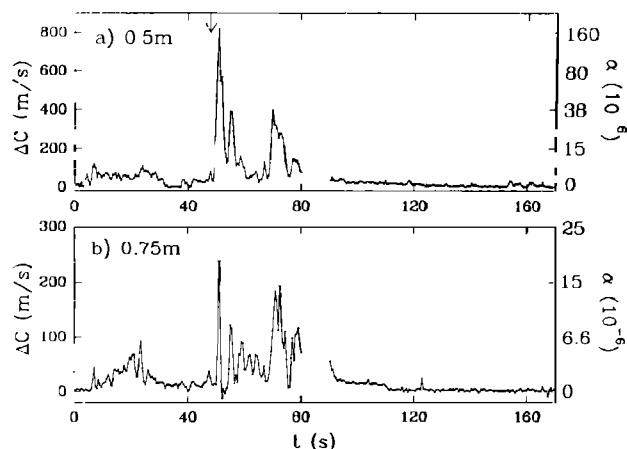


FIG. 9. Highest sound-speed anomalies measured during both experiments at (a) 0.5 m and (b) 0.75 m. The first large peak at approximately  $t=50$  s was caused by a wave which broke at the buoy at the time indicated by the arrow. The second peak approximately 25 s later was caused by a bubble cloud formed 25 s earlier which drifted by the buoy. The void fractions corresponding to the sound-speed anomalies are shown on the right axes. The frequency of the acoustic pulses was 5 kHz. Buzzards Bay data.

most sensor. The deeper sensors were not in the field of view of the camera. Accordingly, large sound-speed anomalies up to 800 m/s were measured immediately after the beginning of breaking in Fig. 9. Less than a second prior to this breaking event, another large breaking wave was observed some meters ahead of the buoy. It is not clear whether these two separate breaking events were from two different waves breaking almost simultaneously or whether they were from the same wave crest breaking at two different locations along the crest. In any case, the important observation to retain is that a second bubble plume was formed some distance away from the buoy and was clearly seen to drift toward the buoy. Approximately 25 s later, this second bubble cloud eventually drifted by the buoy and at that time, an appreciably higher bubble density was observed on the video. Concurrently, the sound-speed anomaly increased significantly during the passage of this second cloud. Thus it would appear that even relatively "older" clouds which have had plenty of time to degas, 25 s in this case, still contain air concentrations high enough to cause anomalies up to 400 m/s.

### E. Dependence of the sound-speed anomaly on the acoustic frequency

Because of the high variability of the sound-speed measurements, it is difficult to adequately compare measurements made at different frequencies unless the measurements are simultaneous. Consequently, a broadband pulse was used during the Buzzards Bay experiment to measure the sound speed at various frequencies simultaneously. The broadband pulse was synthesized from four different pulses of center frequencies 5, 10, 20, and 40 kHz. The amplitudes of the four individual pulses were adjusted to compensate for the 12 dB/oct response of the omnidirectional hydrophone transmitter. The broadband pulse was therefore obtained by superposing the four single frequency pulses. The transmit and receive broadband pulses were bandpass filtered at selected

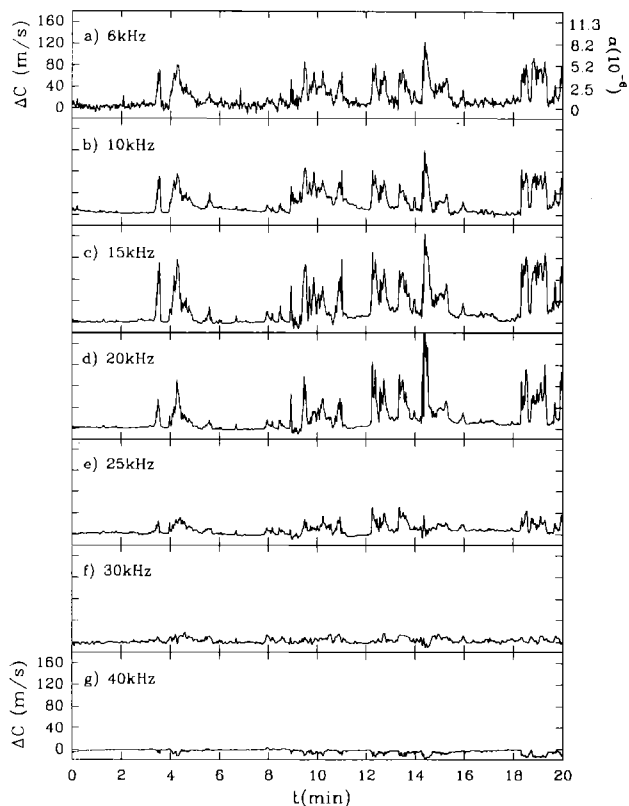


FIG. 10. Sound-speed anomalies at various frequencies obtained by bandpass filtering a 20-min record of broadband pulse data acquired at a depth of 0.5 m. The various bandpass frequencies are indicated on the plots. The axes on the right-hand side show the corresponding void fraction, valid for frequencies below 20 kHz. The wind speed and the SWH were 8 m/s and 0.46 m, respectively. Buzzards Bay data.

frequencies and cross correlated in the usual manner to obtain the time delay and the sound speed at specific frequencies.

The data were bandpass filtered with finite impulse response (FIR) filters. Because of the broadband nature of the transmitted and received pulses, it was possible to filter the broadband pulse at frequencies different from the four principal frequencies and thus obtain sound-speed measurements at several other frequencies. It should also be pointed out that the results presented in this section are insensitive to changes in the shape of the bandpass filters as long as the filter characteristics remain similar (i.e., same center frequency and a relatively tight bandpass region).

Time series of the sound-speed anomaly at various frequencies are obtained by bandpass filtering a record of broadband pulse data at various frequencies from 6 to 40 kHz. After bandpass filtering, the pulses are cross correlated in the usual manner to obtain the time delay and hence the sound-speed anomaly. Figure 10 shows simultaneous time series of sound-speed anomalies at various frequencies. Although energy was contained at frequencies as low as 5 kHz in the transmit pulse, the received signal only contained energy above the noise level from 6 kHz up to approximately 40 kHz. The signal in Fig. 10 shows large intermittent fluctuations which are caused by bubble clouds being advected by the sensors. The signals are highly correlated and of similar magnitude up to approximately 20 kHz. Beyond 20 kHz,

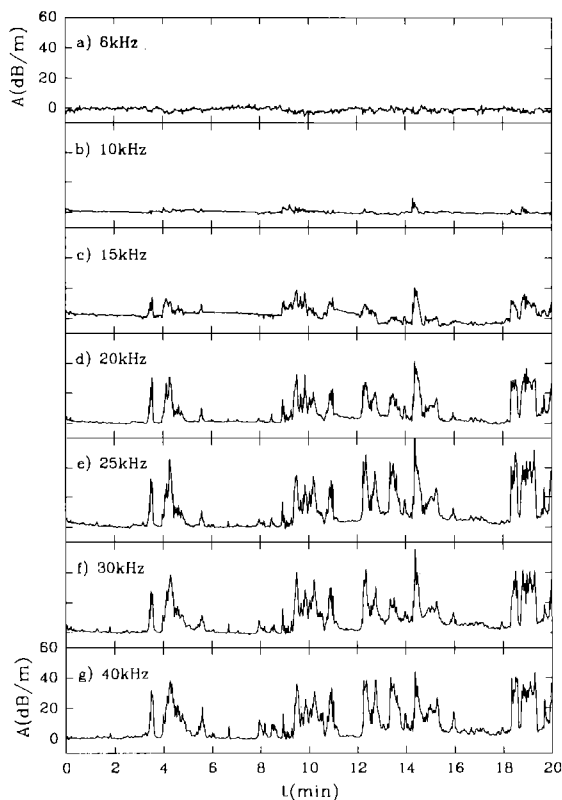


FIG. 11. Received amplitude signal at various frequencies obtained by bandpass filtering a 20-min record of broadband pulse data acquired at a depth of 0.5 m. The various bandpass frequencies are indicated on the plots. The wind speed and the SWH were 8 m/s and 0.46 m, respectively. Buzzards Bay data.

the signals are still correlated but their magnitudes change drastically.

At 40 kHz, the sound-speed anomalies become negative with the sound speed slightly increasing inside the bubble clouds. This behavior is probably caused by a local inhomogeneity in the bubble population such as a local peak or a change in the slope of the power law characterizing the bubble density. Such local features can generate significant sound-speed augmentation or reduction depending on whether the frequency of the sound wave is above or below the resonance frequency corresponding to the bubble size where the inhomogeneity is located. Indeed, such behavior has been observed in the past at a similar frequency (40 kHz) and was believed to be caused by a local peak in the bubble population.<sup>20,21</sup>

The similarity in the structure and amplitude of the signals below 20 kHz suggest that the sound speed is not a function of frequency in that range and thus the fluctuations are caused by the void fraction and not by phase shifts caused by bubble resonance. The nondispersive nature of sound below 20 kHz justifies the use of Wood's equation for calculating the corresponding void fraction [refer to the right axis in Fig. 10(a)]. Starting at 20 kHz, the sound-speed reductions caused by the void fraction are still present but the effect of bubble resonance on the sound speed become more important and they start to alter the signal significantly as the frequency increases above 20 kHz. Notice that features in the

signal caused by the void fraction at low frequencies are well correlated with features at high frequencies which are due mostly to bubble resonance (for example the negative features 40 kHz). This was to be anticipated since the sound-speed fluctuations caused either by the void fraction or by bubble resonance must always coincide with the presence of a bubble cloud at the sensors.

It is also of interest to compute the amplitude of the received acoustic pulses relative to the signal amplitude in bubble-free water which is obtained at a low sea state. After bandpass filtering the broadband pulses, the amplitude is computed by measuring the maximum peak-to-peak amplitude of the received bandpass signal. {The amplitude data are not absolutely calibrated since amplitude fluctuations may result from both attenuation in the bubbly fluid and modulations in the electroacoustic efficiency of the transmitters with changes in the acoustic impedance of the medium. We have observed in lake trials that the amplitude of the signal slightly increased with a reduction in the sound speed. This explains the small positive fluctuations (increases in amplitude) which are correlated with the presence of bubble clouds in the 6 kHz amplitude measurements [Fig. 11(a)]. The data from Fig. 11(a) also suggests that the effect caused by a change in the impedance of the medium is relatively small, at least for low frequencies.} Figure 11 shows time series of the amplitude (relative to that in bubble-free water) for the same data record as the sound-speed anomaly measurements shown in Fig. 10. The similarities between the two figures are striking. The high-frequency reduction in amplitude (say above 15 kHz) complements the sound-speed anomalies at low frequencies (say below 20 kHz). At high frequencies, the acoustic pulses begin to excite bubbles into resonance and this causes increased attenuation of the signal. This is a well-known effect which has been observed by many investigators studying bubbly flows and a good review of measurements and theory can be found in Commander and Prosperetti.<sup>10</sup> Herwig and Nutzel<sup>26</sup> have measured similar time series of attenuation at these frequencies for stronger wind conditions and greater depth. They have also observed greater attenuation with increasing frequencies consistent with the data presented in Fig. 11.

The average of the sound-speed time series shown in Fig. 10 were computed at all frequencies and the results are shown in Fig. 12 (circular symbols). As expected from the previous analysis of the time series, the average sound-speed anomaly  $\overline{\Delta c}$  is almost independent of frequency at frequencies below 20 kHz. Thus the data show that the low-frequency asymptotic limit which occurs when the sound speed is solely dependent on the void fraction is reached for frequencies below 20 kHz at a wind speed of approximately 8 m/s. However, it is likely that this limit will be a function of the sea state and that at higher sea states the limit may be at a lower frequency since more larger bubbles are likely to be present below the surface in these conditions. At frequencies above 20 kHz, the average sound-speed anomaly decreases rapidly and it becomes slightly negative at 35 and 40 kHz.

The standard deviations of the sound-speed anomaly  $\sigma_{\Delta c}$  are shown as triangular symbols in Fig. 12. It is interesting to

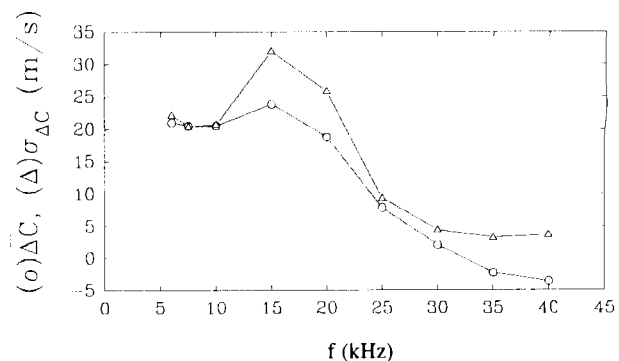


FIG. 12. (○) Average sound-speed anomaly  $\overline{\Delta c}$  and (△) standard deviation  $\sigma_{\Delta c}$  as a function of frequency. The averages and standard deviations were computed over the 20-min time series shown in Fig. 10. Note how  $\overline{\Delta c}$  is almost independent of frequency below 20 kHz.

notice that the magnitude of the standard deviations for the sound-speed anomalies are comparable to the averages. This emphasizes the importance of the short-term fluctuations and it shows that characterization of the sound-speed signal in terms of averages only may not always be appropriate. Note that the peak in  $\sigma_{\Delta c}$  at 15 kHz also corresponds to an increase in  $\overline{\Delta c}$  (Fig. 12) at the same frequency. The reason for this may be that signal fluctuations increase at the transition zone where dispersive effects begin.

Although the magnitude of the averages and standard deviations of the sound-speed anomalies were shown to be similar at low frequencies (10 kHz and below), it is interesting to compare their probability distributions in order to verify the similarity of the signal structure. Figure 13(a) shows the cumulative probability distributions of the sound-speed anomalies at 0.5 m for the frequencies 6, 7.5, and 10 kHz. Notice that all three distributions are very similar indicating that the structure of the signals at low frequencies are also similar. By contrast, Fig. 13(b) shows that the distributions are very different if the selected frequencies extend over the low and high frequency region.

## F. Comparison between sound-speed and upward-looking sonar measurements

Many studies of bubbles in the upper ocean have been conducted using upward-looking sonars (see Thorpe<sup>27</sup> for a recent review). In order to qualitatively compare the measurements of sound speed presented in this paper with previous sonar studies, an upward-looking sonar was mounted at the bottom of the buoy and operated simultaneously with the other instrumentation. The (uncalibrated) sonar is a Furuno model FCV-561 with an 88-kHz center frequency and 11° beamwidth. It was operated with a repetition rate of 10 Hz and the pulse envelopes were stored on a DAT recorder. The sonar was mounted at a depth of 3.5 m and was looking at 22° off the vertical in order to avoid scattering from the structural elements of the buoy. Accordingly, the footprint of the sonar on the surface was approximately 0.7 m in diameter and offset by 1.4 m from the buoy's vertical

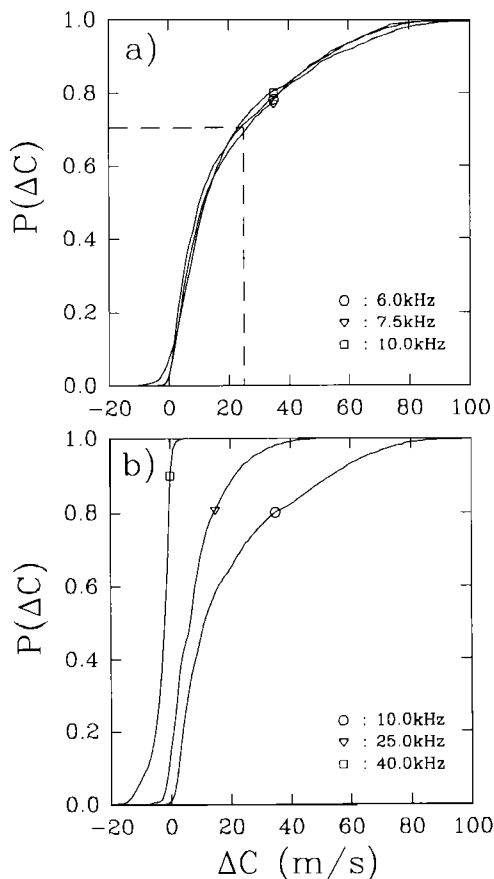


FIG. 13. Cumulative probability distributions of the sound-speed anomaly at a depth of 0.5 m for (a) three low frequencies and (b) three different frequencies spanning the full frequency range. The dashed line shows that 30% of the time the signal was above 24 m/s. Distributions from data shown in Fig. 10.

centerline. Thus the sonar and the sound-speed instrumentation were slightly offset horizontally with a maximum offset of 1.2 m at a depth of 0.5 m.

Figure 14(a) shows sonar power backscatter data as a function of depth and time for a wind speed of 8 m/s and a significant wave height of 0.46 m. Note that the backscatter data are not calibrated. The gray scale intensity from white to black spans a 64-dB range. Bubble clouds drifting through the sonar beam are clearly identifiable as whiter structure extending down, in some instances, to a depth of 3.25 m. This bubble cloud image is very similar to what has been presented in other sonar studies.<sup>1-3,27</sup> The water surface is also clearly identified by the white contour although it is evident that with a single frequency sonar it becomes difficult and arbitrary to decide where the surface is located especially at times when backscatter from bubble clouds smear the usually sharp surface backscatter which occurs in bubble-free conditions.

Sound-speed anomalies were measured simultaneously with the sonar backscatter and are shown in Fig. 14(b), (c), (d) for depths corresponding to 0.5, 0.75, and 1.0 m. As expected, the presence of bubble clouds at the buoy corresponds well with an increase in the sound-speed anomaly. Perhaps more surprising is the fact that no sound-speed anomalies were measured above the noise level ( $\pm 2$  m/s) at

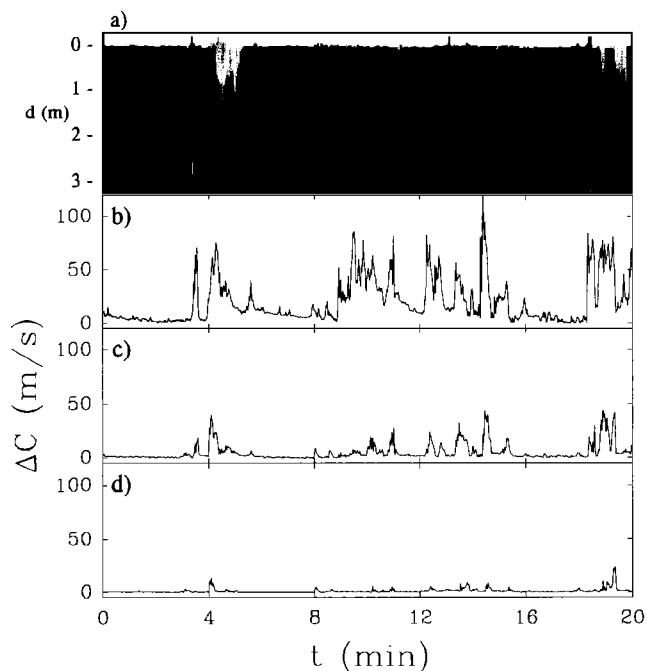


FIG. 14. (a) Sonar backscattered power data as a function of depth and time. (b), (c), (d) Corresponding time-series of sound-speed anomalies at a depth of (b) 0.5 m, (c) 0.75 m, and (d) 1.0 m. The sound-speed anomalies are from the same data record as Fig. 10 for the 10-kHz data. The wind speed and significant wave height were 8 m/s and 0.46 m, respectively. Buzzards Bay data.

a depth of 1.5 m and greater although bubble clouds were clearly present down to at least 3.25 m. This, of course, indicates the greater sensitivity of high-frequency sonars to bubbles; but it also shows that from a sound-speed point of view, the significant anomalies are located very close to the surface (within 1 m at 8 m/s wind speed) even though clouds of bubbles are detected by sonars down to several meters.

#### IV. DISCUSSION AND CONCLUSION

We have reported on the results from two field experiments on the measurement of sound speed near the ocean surface. The most significant novelties of the present measurements are that they are taken simultaneously at several different depths, starting as close as 0.5 m, and over a frequency range from 5 to 40 kHz. Furthermore, the technique for measuring the speed of sound is a direct one which avoids the many difficulties involved with inferring sound speed from *in situ* void fraction or bubble population measurements. Although the measurements are limited to moderate wind conditions (8 m/s or less), they have nevertheless furnished surprising results on the characteristics of the sound-speed signals close to the ocean surface.

First and foremost, at acoustic frequencies below 20 kHz for which the sound speed was shown to be nondispersive, time series of the sound-speed anomaly and received signal amplitude showed dramatic fluctuations over intervals of seconds to minutes. The large fluctuations measured were attributed to higher void fraction found in bubble plumes and clouds advected by the sensors. In two particular instances, a newly created bubble plume generated a sound-speed anomaly of 800 m/s at 0.5 m, and a bubble cloud 25-s old

generated an anomaly of 400 m/s. At a wind speed of 8 m/s, we have observed many [ $O(10)$ ] sound-speed anomalies above 100 m/s in 20-min time series at a depth of 0.5 m. These are the first reported time series of sound-speed anomalies in the shallow ocean surface layer and the fluctuations measured are two to three orders of magnitude greater than previously reported measurements averaged over 10 to 20 min.<sup>2,20,21</sup> Sound-speed anomalies above the noise level of the instrument ( $\pm 2$  m/s) were seldom observed at a depth of 1.5 m, and never at 2.0 m for 8 m/s wind conditions.

The sound-speed anomalies at various depths were found to be highly correlated and mostly coherent at frequencies below 0.05 Hz which corresponded to the frequency region where the signal was most energetic. At a wind speed of 8 m/s and SWH of 0.5 m, the time-averaged sound-speed anomaly was found to decrease exponentially with depth with an  $e$ -folding depth of 0.18 m and an extrapolated anomaly at the surface of 370 m/s. In contrast, Farmer and Vagle<sup>2</sup> have measured an exponential profile with an  $e$ -folding depth of 1.4 m and an anomaly at the surface of 3 m/s in wind conditions of 10 m/s (and unreported significant wave height). The present measurements indicate that the sound-speed anomaly profile may be significantly more pronounced (by two orders of magnitude) and shallower (by one order of magnitude) than previously reported by Farmer and Vagle.<sup>2</sup>

While some of the differences with the measurements of Farmer and Vagle's<sup>2</sup> are probably due to variations in the environmental conditions, most of the differences may be due to difficulties in inferring sound-speed anomalies from bubble population measurements.<sup>22,23</sup> Farmer and Vagle<sup>2</sup> have computed the time-averaged sound-speed profile by integrating the dispersive effects of bubbles using a well-known integral equation which takes as input the measured bubble size distribution. For their study, they used measurements at four discrete radii (16, 37, 65, and 116  $\mu\text{m}$ ) to infer the shape of the bubble population which can usually be described by power laws. The integral equation for determining the sound speed from bubble population can be very sensitive to the exact value of the exponents of these power laws and to the upper and lower bubble size limits on the integral itself. For example, Farmer and Vagle<sup>2</sup> have measured a slope between  $a^{-4}$  and  $a^{-6}$  above a bubble radius of 60  $\mu\text{m}$  while many investigators have found slopes between  $a^{-2.5}$  and  $a^{-3}$  (refer to Lamarre and Melville<sup>22</sup> for details and references). Such differences can yield errors by factors of 3 or 4 in the calculation of sound speed using the integral equation.<sup>22</sup> Variations in the position of the peak of the bubble population (say between 16 and 24  $\mu\text{m}$ ) can yield a further difference by a factor of 2. Variations in the upper limit of the integral equation can generate even greater discrepancies especially when the slope of the bubble population is small<sup>23</sup> (say  $a^{-2.5}$  to  $a^{-3.5}$ ). Thus it is clear that sound-speed calculations based on integration of bubble population data are very sensitive to the exact shape of the bubble size distribution and the location of its upper and lower limits for which there are still large discrepancies in the literature.

Another possible cause for the differences with Farmer and Vagle's<sup>2</sup> measurements is the difficulty in differentiating

between surface scattering and scattering by the dense bubble layer immediately below the surface when using a sonar technique. This is especially true close to the water surface. Another possibility may be that their measurements, which were performed with a sonar located 20 to 30 m away from the surface, were not exactly at the depth reported. The present study has shown that small differences in measurement depth on the order of 10 to 50 cm can make an important difference in the magnitude of the signal measured. Other possibilities also include the complex issue of multiple scattering which is not taken into account with the sonar technique and which may become significant near the surface where the bubble density is important. Finally, we point out that the spot size of the sonar beam at low frequencies will affect its resolution of the surface and it may become difficult, at low enough frequencies, to effectively locate the crest and the trough of the waves (for example, a 28-kHz sonar with an 18° beam width and located at a depth of 30 m will have a spot size on the surface of 9.4 m).

Medwin and his co-authors<sup>20,21</sup> measured average sound-speed anomalies up to 15 m/s at a depth of 3 m during light wind conditions (approximately 3 m/s) while our measurements show that sound-speed anomalies above 1 m/s are confined to the first meter below the surface for an 8 m/s wind speed. We believe that the greater sound-speed anomalies measured by Medwin<sup>20</sup> and Medwin *et al.*<sup>21</sup> were due to enhanced breaking on the offshore platforms from which they made their measurements.

The sound-speed anomaly was found to agree relatively well with an exponential probability distribution where the probability of occurrence of large anomalies decreased exponentially with the magnitude of the anomaly. As anticipated, the exponential decrease was found to be significantly greater with depth since the probability of finding a large sound-speed anomaly at greater depth is smaller. The exponential decrease of the probability distribution was also found to be greater at low sea state and thus as one would expect, large sound-speed anomalies are less likely to be found in calmer sea conditions.

The average (20 min) sound-speed anomaly at a depth of 0.5 m was found to increase with wind speed. The average anomalies were found to start increasing at wind speeds in the range 2 to 3 m/s which is consistent with the wind speed threshold for the onset of observable wave breaking in the ocean. At a wind speed of 8 m/s, the average sound-speed anomaly was approximately 20 to 25 m/s and the extrapolation of the correlation up to 15 m/s suggest that the average anomaly at a depth of 0.5 m would be around 40 to 50 m/s for these often-encountered wind conditions.

The measurement technique presented in detail in Lamarre<sup>23</sup> and Lamarre and Melville<sup>22</sup> was expanded to include simultaneous measurements of the sound speed at multiple frequencies ranging from 6 to 40 kHz. The technique makes use of a broadband pulse which was bandpass filtered at various frequencies and cross correlated to extract the sound speed and received signal amplitude at the various frequencies. The technique could easily be improved to include real-time bandpass filtering and a much higher upper frequency range (up to 100 kHz). The results obtained

showed that the sound-speed anomaly became nondispersive below 20 kHz. Above 20 kHz, the signal becomes dispersive and rapid changes in the sound-speed anomalies have been observed between 20 and 30 kHz. At higher frequencies (35 and 40 kHz), the average sound-speed anomaly became slightly negative indicating that the propagation velocity was increasing from its bubble-free value. The amplitude measurements at high frequencies (above 15 kHz) were found to complement the sound-speed anomalies at low frequencies (below 20 kHz) at all measurement depths. It is the passage of bubble clouds which generates both the sound-speed anomaly and the modulations in the signal amplitude and thus it is not surprising that the structure of both signals are complementary.

In our effort to understand the reasons for the rapid decrease in the average sound-speed anomalies between 20 and 30 kHz we have determined the shape of the bubble population from our measurement of sound-speed anomalies (Fig. 12).<sup>23</sup> This is referred to as the "inverse" problem. The "forward" problem being the calculation of sound-speed anomalies from bubble population measurements.<sup>9,10</sup> The result of this modeling effort suggest that the rapid decrease is caused by a transition in the slope of the bubble population from  $a^{-3}$  to  $a^{-6}$  occurring at a bubble size of approximately 160  $\mu\text{m}$ . It should be pointed out that previous studies of bubble population at sea have reported slopes of  $a^{-3}$  for bubble sizes above 60  $\mu\text{m}$ . However, this slope must necessarily become steeper than  $a^{-3}$  at some larger bubble size in order to keep the amount of air in the water finite. Our modeling effort suggest that such a transition occurs around 160  $\mu\text{m}$  where the slope becomes  $a^{-6}$ . This conclusion is for an 8-m/s wind speed. It is likely that the transition bubble size is greater at higher wind speeds since more large bubbles would be entrained by breaking.

Finally, an upward-looking sonar revealed the presence of bubble clouds which were found to correlate with large increases in the sound-speed anomaly. However it was found that although the sonar showed clouds extending down to a depth of 3 m and greater at a wind speed of 8 m/s, the significant sound-speed reductions and high void fractions were confined to the first meter below the surface.

## ACKNOWLEDGMENTS

We thank Dr. Anatol Rozenberg and Mr. Alexey Fedorov for their invaluable assistance during the field experiments. The upward-looking sonar system was deployed and operated by Dr. Rozenberg. We also thank Dr. Albert Williams III who has provided helpful advice in the developmental stage of the instrument. This work is supported by the Office of Naval Research (Ocean Acoustics).

<sup>1</sup>S. A. Thorpe, "On the clouds of bubbles formed by breaking waves in

deep water and their role in air-sea gas transfer," *Philos. Trans. R. Soc. London A* **304**, 155–210 (1982).

- <sup>2</sup>D. M. Farmer and S. Vagle, "Waveguide propagation of ambient sound in the ocean surface bubble layer," *J. Acoust. Soc. Am.* **86**, 1897–1908 (1989).
- <sup>3</sup>L. Zedel and D. Farmer, "Organized structures in subsurface bubble clouds: Langmuir circulation in the open ocean," *J. Geophys. Res.* **96**, 8889–8900 (1991).
- <sup>4</sup>E. Lamarre and W. K. Melville, "Instrumentation for the measurement of void-fraction in breaking waves: laboratory and field results," *J. Ocean. Eng.* **17**, 204–215 (1992).
- <sup>5</sup>F. S. Henyey, "Acoustic scattering from microbubble plumes in the 100 Hz to 2 kHz region," *J. Acoust. Soc. Am.* **90**, 399–405 (1991).
- <sup>6</sup>D. K. Woolf and S. A. Thorpe, "Bubbles and the air-sea exchange of gases in near-saturation conditions," *J. Marine Res.* **49**, 435–466 (1991).
- <sup>7</sup>D. W. R. Wallace and C. D. Wirick, "Large air-sea gas fluxes associated with breaking waves," *Nature* **356**, 694–696 (1992).
- <sup>8</sup>A. B. Wood, *A Textbook of Sound* (Bell, London, 1941), pp. 360–362.
- <sup>9</sup>C. S. Clay and H. Medwin, *Acoustical Oceanography* (Wiley, New York, 1977).
- <sup>10</sup>K. W. Commander and A. Prosperetti, "Linear pressure waves in bubbly liquids: Comparison between theory and experiments," *J. Acoust. Soc. Am.* **85**, 732–746 (1989).
- <sup>11</sup>S. Vagle, W. G. Large and D. M. Farmer, "An evaluation of the WOTAN technique of inferring oceanic winds from underwater ambient sound," *J. Atmos. Oceanic Tech.* **7**, 576–595 (1990).
- <sup>12</sup>J. A. Nystuen, "Rainfall measurements using underwater ambient sound," *J. Acoust. Soc. Am.* **79**, 972–982 (1986).
- <sup>13</sup>F. Laville, G. D. Abbott, and M. J. Miller, "Underwater sound generation by rainfall," *J. Acoust. Soc.* **89**, 715–721 (1991).
- <sup>14</sup>L. Ding, "Acoustical studies of breaking waves in the open ocean," Ph.D. thesis, University of Victoria & Institute of Ocean Science, Victoria, B. C., Canada (1992).
- <sup>15</sup>W. K. Melville, M. R. Loewen, F. C. Felizardo, A. T. Jessup, and M. J. Buckingham, "Acoustic and microwave signatures of breaking waves," *Nature* **336**, 54–59 (1988).
- <sup>16</sup>M. R. Loewen and W. K. Melville, "Microwave backscatter and acoustic radiation from breaking waves," *J. Fluid Mech.* **224**, 601–623 (1991).
- <sup>17</sup>F. C. Felizardo and W. K. Melville, "The correlation between wave energy dissipation and ambient noise in the ocean," *Proceedings of A Symposium on the Air-Sea Interface*, Marseilles, France (1993) (in press).
- <sup>18</sup>E. Lamarre and W. K. Melville, "Air entrainment and dissipation in breaking waves," *Nature* **351**, 469–472 (1991).
- <sup>19</sup>M. J. Buckingham, "On acoustic transmission in ocean-surface waveguides," *Philos. Trans. R. Soc. London Ser. A* **335**, 513–555 (1991).
- <sup>20</sup>H. Medwin, "Acoustic fluctuations due to microbubbles in the near-surface ocean," *J. Acoust. Soc. Am.* **75**, 1100–1104 (1974).
- <sup>21</sup>H. Medwin, J. Fitzgerald, and G. Rautman, "Acoustic miniprobing for ocean microstructure and bubbles," *J. Geophys. Res.* **80**, 405–413 (1975).
- <sup>22</sup>E. Lamarre and W. K. Melville, "Instrumentation for the measurement of sound-speed near the ocean surface," *J. Atm. Oceanic Tech.* (in press).
- <sup>23</sup>E. Lamarre, "An experimental study of air entrainment by breaking waves," Ph.D. thesis, Massachusetts Institute of Technology and Woods Hole Oceanographic Institution, Massachusetts (1993).
- <sup>24</sup>V. A. Del Grosso, "New equation for the speed of sound in natural waters (with comparisons to other equations)," *J. Acoust. Soc. Am.* **56**, 1084–1091 (1974).
- <sup>25</sup>H. Medwin, "Speed of sound in water: a simple equation for realistic parameters," *J. Acoust. Soc. Am.* **58**, 1318–1319 (1975).
- <sup>26</sup>H. Herwig and B. Nutzel, "The influence of bubbles on acoustic propagation and scattering," in *Underwater Acoustic Data Processing*, edited by Y. T. Chan (Kluwer, Dordrecht, 1989), pp. 105–111.
- <sup>27</sup>S. A. Thorpe, "Bubble clouds and the dynamics of the upper-ocean," *Q.J.R. Meteorol. Soc.* **118**, 1–22 (1992).